Neutron capture cross sections on ^{138}Ba, ^{140,142}Ce, ^{175,176}Lu, and ^{181}Ta at 30 keV: Prerequisite for investigation of the ^{176}Lu cosmic clock

H. Beer and F. Käppeler

Kernforschungszentrum Karlsruhe GmbH, Institut für Angewandte Kernphysik, Postfach 3640, D-7500 Karlsruhe, Federal Republic of Germany

(Received 2 October 1979)

The capture cross sections of ^{138}Ba, ^{140,142}Ce, ^{176}Lu, ^{181}Ta and the capture cross section of ^{175}Lu to the 3.68 h isomeric state in ^{176}Lu have been determined at 30 keV neutron energy using the activation technique. Neutrons were generated via the ^{7}Li(p,n) reaction just above the reaction threshold at a 3 MV pulsed Van de Graaff accelerator. The capture cross sections are of importance to stellar nucleosynthesis. With the ^{138}Ba and ^{140}Ce cross sections the time integrated average neutron flux for the s process was determined to 0.22 mb^{-1}. This result, the capture cross section of ^{176}Lu and the ^{175}Lu cross section to the 3.68 h isomeric state in ^{176}Lu were used to analyze the ^{176}Lu cosmic clock. The mean s process age of solar matter before the solidification of the solar system was estimated to 6×10^{9} yr. In addition the Hf/Lu abundance ratio was determined.

[NUCLEAR REACTIONS ^{138}Ba(n,γ), ^{140,142}Ce(n,γ), ^{175}Lu$(n,\gamma)^{176}$Lu^{m}, ^{176}Lu(n,γ), ^{181}Ta(n,γ); E_n=30 keV; measured capture cross sections; nucleosynthesis; ^{176}Lu cosmochronometer, Hf and Zr abundances.]

INTRODUCTION

For the determination of the age of the universe methods associated with nucleosynthesis represent an important alternative to the techniques offered by astronomical observations. Up to now, all attempts to investigate cosmic clocks from the analysis of the time dependent abundances of long-lived unstable nuclei concerned isotopes produced in the rapid neutron capture process or r process.[1-3] We have started to investigate the ^{176}Lu clock which is unique as it is the only suitable isotope generated by the slow neutron capture process (s process). Consequently, this age determination may yield another independent piece of information about our galactic evolution. The s process has the further advantage that relevant quantities are normally accessible to laboratory measurements because the nuclei are synthesized along the valley of stability where mostly stable isotopes are involved.

In theoretical studies of this chronometer it has been emphasized that only accurate experimental capture cross sections allow for a meaningful analysis.[4-6] Especially the population of the 3.68-h isomeric state in ^{176}Lu via neutron capture in ^{175}Lu must be determined with high precision. As there were no such data available, we started a first series of measurements using an activation technique. With a pulsed 3 MV Van de Graaff accelerator, we were able to produce a neutron spectrum similar to a Maxwellian energy distribution for a thermal energy of $kT \sim 30$ keV via the ^{7}Li(p,n) reaction. This temperature is expected for the s-process environment. In this neutron spectrum cross-section measurements were performed for the reactions ^{138}Ba$(n,\gamma)^{139}$Ba, ^{140}Ce$(n,\gamma)^{141}$Ce, ^{142}Ce$(n,\gamma)^{143}$Ce, ^{175}Lu$(n,\gamma)^{176}$Lu^{m}, ^{176}Lu$(n,\gamma)^{177}$Lu, and ^{181}Ta$(n,\gamma)^{182}$Ta. The capture cross section of ^{175}Lu to the short-lived isomeric state ^{176}Lu^{m} can be measured only by activation.

Beside the special neutron spectrum, the activation technique used is characterized by the following features:

(a) The activation samples were placed very close to the neutron target in a comparably high flux. Thus it was possible to measure the small cross sections of ^{138}Ba and ^{140}Ce accurately even with small amounts of sample material. In every case, only thin samples were used to minimize corrections for scattering or self-absorption effects.

(b) The method is so sensitive that no high isotopic enrichments are required. This allows even the investigation of the rare isotope ^{176}Lu with a natural Lu sample.

(c) All measurements are carried out with a ^{197}Au foil as a standard which is activated simultaneously. In this way most systematic uncertainties can be avoided.

(d) The neutron flux during the activation is recorded continuously to account for the exact activation history.

(e) All samples are counted with a calibrated high resolution Ge(Li) detector to achieve the best signal-to-background ratio.

 © 1980 The American Physical Society

With this technique we have determined an accurate and consistent set of cross sections which allowed a first analysis of the ^{176}Lu clock and of some connected problems.

EXPERIMENTAL METHOD

The neutron activation technique consists of two steps: neutron irradiation of a suitable sample and absolute counting of the induced activity. In principle this seems to be a relatively simple method for the determination of a neutron capture cross section. However, it is known from literature that severe uncertainties may arise unless all steps are performed with extreme care.

Figure 1 shows schematically how the irradiations were carried out. The ^{7}Li(p,n) reaction was used for neutron production with proton energies just above the reaction threshold. In this way all neutrons generated are kinematically collimated in a forward cone with an opening angle of 120°. This important feature prevents any disturbing scattering of the primary neutron beam in the vicinity of the samples. The copper target backing of 0.5 mm thickness represents the only source of scattered neutrons. As the transmission through the backing is 96% in the energy range of interest, neutron scattering causes only a small effect. In addition the locus of the scattering events is identical with the neutron target and the spectrum of scattered neutrons is practically unchanged. Therefore it is obvious that neutron scattering can be neglected completely in our case. This was also checked experimentally, by placing In foils on the target backing but outside the neutron cone. No activity from activation by scattered neutrons was found at a detectable level. From all this it was estimated that any uncertainty introduced by scattered neutrons should be less then 0.2%.

Target cooling was achieved by lateral heat conduction in the Cu backing to a water cooled ring of 8 mm inner diameter. The Li target itself was an evaporated metallic layer 6 mm in diameter. The beam spot of 1-mm size was swept magnetically across the target in order to defocus the beam and to achieve a homogeneous illumination of the target. With this arrangement beam currents up to 150 μA can be tolerated.

As activation measurements were normally performed with the accelerator beam in dc mode, it was very important to obtain reliable information about the neutron spectrum. In our case all irradiations were carried out in a standard neutron field which was obtained by bombarding thick metallic Li targets with protons of 1.911 MeV, corresponding to a maximum neutron energy of 106 keV and a maximum neutron emission angle of 60°.

This standard spectrum has been investigated by means of the ^{6}Li-glass detector as shown in Fig. 1. Operating the accelerator in pulsed mode with a repetition rate of 1 MHz and a pulse width of 10 ns it was possible to measure the neutron spectrum by the time-of-flight technique. A 90-cm distance between neutron target and ^{6}Li glass detector allowed for a sufficient resolution of ~10 ns/m. From the known ^{6}Li(n,α) cross section it was thus possible to derive the relative neutron yield per energy interval. Measurements of this distribution were performed in steps of 7.5° for neutron emission angles between 0° and 52.5°. Some results are shown in Fig. 2. All spectra are normalized to the same integrated neutron yield. With increasing angle the relative intensity drops off rapidly and the average neutron energy ap-

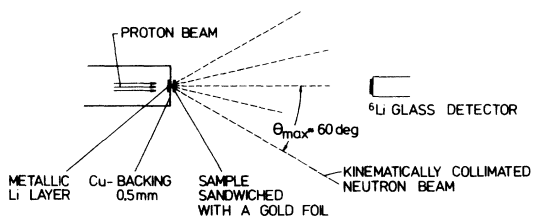

FIG. 1. Scheme of the experimental technique.

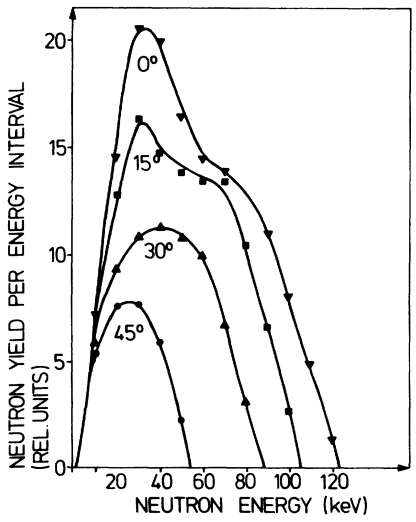

FIG. 2. Neutron yield per energy interval as a function of angle with respect to the proton beam. The yield drops off very rapidly for angles above 55 keV.

proaches the threshold value of 30 keV.

Integration over all angles yields the total neutron spectrum to which the samples are exposed during the irradiations. Figure 4 demonstrates how well this neutron spectrum represents a Maxwellian energy distribution. This enables us to measure directly the Maxwellian averaged cross sections with the activation technique, a possibility which to our knowledge was not considered before. These distributions are discussed further in the following chapter.

Once this standard neutron spectrum was established, it was sufficient to repeat the measurement at 0° before each irradiation to verify the correct maximum neutron energy. Then, without changing the beam energy, the accelerator was put on dc mode for the irradiation. With typical beam currents of 50 to 100 μA a total neutron yield of 10^8–10^9 s^{-1} was obtained. The irradiation history was recorded in a NOVA 2 computer: Besides the irradiation time, the time dependence of the neutron yield was measured also. For that purpose the integral count rate of the ^{6}Li glass detector was stored in intervals of 40 sec. This enabled us to correct for any fluctuations which otherwise could have affected the sample activity with respect to the standard if the respective half-lives were different.

The accuracy of activation measurements depends also critically on the mass of the irradiated samples. In principle the samples should be as thin as possible because then scattering and self-shielding effects are small during the irradiation and during the activity determination afterwards as well. The high neutron flux available allowed us to use sufficiently thin samples. Except for Ba which was a self-supporting carbonate tablet only metallic foils of 6 mm diameter were used with thicknesses between 0.025 and 0.5 mm (for details see Table I). The samples sandwiched with 0.06 mm thick gold foils were attached directly to the target backing. Although natural samples were used, the neutron flux was sufficient to measure even the cross sections of isotopes with low abundance, e.g., ^{176}Lu.

The last step of the experiment is the absolute determination of the induced activity in the investigated sample and in the gold reference sample. The most accurate way for this measurement is high resolution gamma ray spectroscopy with a calibrated Ge(Li) detector. This method guarantees clean background corrections and allows us to sort out the studied nucleus via a characteristic gamma ray line. The gamma spectra from the decay of the samples are recorded as fields of 4096 channels in subsequent time intervals which were considerably shorter than the respective half-lives. This mode of registration has the advantage that an optimum counting time can be chosen from the signal-to-background rations of relevant gamma ray lines. In addition the half-life of the activated nucleus can be determined from the decrease in gamma intensity as a function of time. This represents a check with regard to dead time effects and contaminating activities. As an example, the exponential decrease of the 88-keV gamma line from the 3.68 h activity of the isomeric state ^{176}Lu^m is shown in Fig. 3. The insert demonstrates that the line intensities can be determined very accurately so that the exponential decay curve is well reproduced.

ANALYSIS AND RESULTS

For a particular gamma ray line the number of events C registered in the Ge(Li) detector during the activity determination are given by the expression

$$C = AK_\gamma \epsilon_\gamma f_\gamma (1 - e^{-\lambda T_M}) e^{-\lambda T_W}, \quad (1)$$

TABLE I. Sample characteristics.

Sample	Thickness (mg/cm^2)	Chemical composition	Investigated isotope	Effective thickness for the investigated isotope (mg/cm^2)	(at./b)
Ba	339	$BaCO_3$	^{138}Ba	244	7.46×10^{-4}
Ce	132	metal	^{140}Ce	117	5.05×10^{-4}
			^{142}Ce	14.9	0.633×10^{-4}
	134	metal	^{140}Ce	119	5.13×10^{-4}
			^{142}Ce	15.2	0.643×10^{-4}
Lu	31.6	metal	^{175}Lu	30.8	1.06×10^{-4}
	396	metal	^{176}Lu	10.3	0.353×10^{-4}
Ta	940	metal	^{181}Ta	940	31.31×10^{-4}
Au	112	metal	^{197}Au	112	3.42×10^{-4}

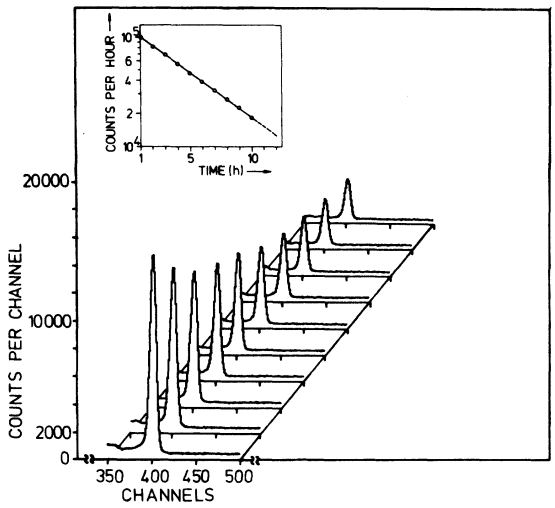

FIG. 3. Gamma ray spectra from the decay of the isomeric state $^{176}Lu^{m}$, taken in intervals of 1 h. The exponential decrease of the 88 keV line is obvious (see insert).

where ϵ_γ is the Ge(Li) efficiency, f_γ the relative gamma intensity per decay for the investigated line, and λ is the decay rate. T_W is the time interval between irradiation and activity measurement and T_M stands for the Ge(Li) measuring time. K_γ gives the correction factor for gamma self absorption in the sample. For disk shaped samples[7] of thickness d one obtains $K_\gamma = 1/d\mu(1 - e^{d\mu})$. The gamma absorption coefficients μ were taken from Ref. 8.

The number of activated nuclei A can be written as

$$A = \phi_T N \sigma f_B . \tag{2}$$

Here, $\phi_T = \int \phi(t)dt$ is the time integrated neutron flux, N the sample thickness in at./b, and σ the capture cross section. The factor

$$f_B = \int_0^{T_B} \phi(t) e^{-\lambda(t-T_B)}\, dt \Big/ \int_0^{T_B} \phi(t)\, dt \tag{3}$$

accounts for the decay of activated nuclei during irradiation time T_B. For a constant neutron flux, f_B reduces to

$$f_B = \frac{1}{\lambda T_B}(1 - e^{-\lambda T_B}) . \tag{3a}$$

As the measurements are carried out relative to ^{197}Au as a standard, the neutron flux ϕ_T cancels out to first order, if the number of activated nuclei is normalized to gold:

$$\frac{A_i}{A_{Au}} = \frac{\sigma_i}{\sigma_{Au}} \frac{N_i}{N_{Au}} \frac{f_{B_i}}{f_{B_{Au}}} . \tag{4}$$

The cross section σ_i determined from Eq. (4) represents an average over the neutron spectrum used during the irradiation:

$$\sigma_{exp} = \int \sigma(E)\phi(E)\, dE \Big/ \int \phi(E)\, dE . \tag{5}$$

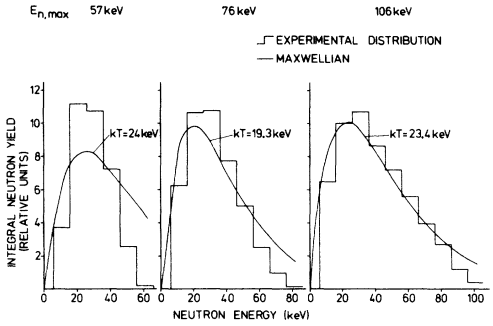

FIG. 4. Integral neutron yields (histogram) for various maximum neutron energies ($E_{n,max}$ = 57, 76, 106 keV corresponding to proton energies 5, 10 and 25 keV above threshold) and least squares fits with Maxwellian distributions (solid line). The appropriate thermal energies kT are indicated.

It was mentioned already that the experimental flux distribution $\phi_{exp}(E)$ is very similar to a Maxwellian energy distribution

$$\phi_{Max}(E) \sim E e^{-E/kT} \tag{6}$$

with thermal energies kT in the 20 to 30 keV range. Figure 4 illustrates how the total neutron spectrum to which the samples are exposed changes with increasing proton energy. At 5 keV above the reaction threshold one obtains an almost symmetric spectrum centered at 30 keV with a maximum neutron energy of 57 keV. Obviously the Maxwellian fit is rather poor. The situation is considerably improved for the two other spectra: 10 keV above threshold the maximum neutron energy is 76 keV and in this case the fit for a thermal energy of 19.3 keV shows already an overlap of 85% with the experimental distribution. The best approach to a Maxwell spectrum was achieved for proton energies 25 keV above threshold corresponding to a maximum neutron energy of 106 keV. Now the overlapping area with a Maxwellian distribution for $kT = 23.4$ keV is 90%. In addition, for this proton energy the total neutron yield is also significantly higher than for the lower energies. A further increase in proton energy leads to the difficulty that the neutron cone widens up rapidly so that background start to be more complicated. Therefore we consider the neutron spectrum obtained 25 keV above threshold to be the best choice for the simulation of a Maxwell spectrum near $kT = 30$ keV.

Although the experimental spectrum does not cover the total range from zero energy to infinity, the resulting correction introduced by the limited energy range is not greater than 3%. This means that the results of our measurement represent already proper Maxwellian averaged cross sections

$$\frac{\langle\sigma v\rangle}{v_T} = \frac{2}{\sqrt{\pi}} \int_0^\infty \sigma(E) E e^{-E/kT} dE \Big/ \int_0^\infty E e^{-E/kT} dE$$
$$\sim \frac{2}{\sqrt{\pi}} \bar{\sigma}_{\text{exp}} . \qquad (7)$$

In this expression v_T is the most probable thermal velocity and $2/\sqrt{\pi}$ is a normalization factor introduced by the definition $\langle\sigma v\rangle/v_T$.[9]

All corrections and uncertainties are listed in Table II. Beside the uncertainty from the Au standard cross section the major difficulties arise from the irradiation history and from the extrapolation of the measured cross sections from the experimental neutron spectrum to the "normal" Maxwellian distribution for $kT = 30$ keV. Nevertheless, with the overall uncertainty of 5% to 7% a considerable improvement is achieved compared to existing data.

In Table III the results are shown for all isotopes together with the respective half-lives, the detected gamma-ray energies and intensities. The information on half-lives and decay schemes was taken from the most recent Nuclear Data Sheets (Status 6/79). Only the relative gamma intensity for the 88-keV line in the decay of $^{176}Lu^m$ is taken from a recent measurement of Morel.[10] These values are helpful to understand the quoted uncertainties. For instance, the uncertainty in decay scheme is largest for $^{176}Lu(n,\gamma)^{177}Lu$. But, on the other hand, the associated gamma ray energy is comparably large so that self absorption is small and the half-life is long enough so that the irradiation history is not crucial. Hence, a total uncertainty of 5% is found for this cross section. The fact that statistical uncertainties are not significant at all is illustrated by the comparable accuracies of the very small cross sections of Ba and Ce.

The respective average gold cross sections were calculated using the evaluated file from ENDF/B-IV.[11] The energy dependence of the cross sections which is required for the extrapolation to the "normal" distribution at 30 keV was taken from theoretical work.[12] For the partial capture cross section to the isomeric state $^{176}Lu^m$ no such information was available.

Beside the important isotopes of Ba, Ce, and Lu, the well-known cross section of ^{181}Ta was included in the measurements to give an additional confirmation of the experimental accuracy. Our cross section of 960 ± 50 mb is in good agreement with the 982 mb adopted by Newman.[13]

A comparison of our data with existing values is made in the last two columns of Table III. Especially for the Ce and Ba isotopes the results reported in the literature show large discrepancies, demonstrating the difficulties encountered in the measurement of small cross sections. Here, the advantages of our improved activation technique are outstanding: High neutron flux, small samples, no corrections for scattered neutrons, high resolution gamma spectroscopy and a well-known neutron spectrum which yields Max-

TABLE II. Corrections and uncertainties.

	Correction (%)	Uncertainty (%)
Au standard	···	2.5
Uncertainty in decay scheme	···	0.8–4.0
Ge(Li) efficiency	···	<1.5
Statistics	···	≲1.0
Gamma self absorption in the sample	2–10	0.4–2.0
Activation via scattered neutrons	···	<0.2
Multiple scattering and self shielding	1–2	<0.2
Irradiation history	≲5	<3.0
Deviation of flux distribution from Maxwellian spectrum	≲3	<1.0
Extrapolation of average cross section from $kT = 24$ to 30 keV	···	≲3.0
Total uncertainty		5–7

TABLE III. The relevant decay parameters and the resulting Maxwellian average cross sections.

Reaction	Half-life	Detected gamma transition (keV)	Relative intensity per decay (%)	Fitted thermal energy kT (keV)	Experimental average cross section (mb)	Extrapolated cross section for kT = 30 keV (mb)	Other work (mb)
^{138}Ba$(n,\gamma)^{139}$Ba	82.7 m	165.85	23	23	4.55 ± 0.23	4.22 ± 0.25	8 ± 2 [a] 11 ± 1.5 [b] 5.7 ± 0.9 [c] 3.9 ± 0.8 [d]
^{140}Ce$(n,\gamma)^{141}$Ce	32.51 d	145.44	48.44 ± 0.41	24	12.63 ± 0.57	11.52 ± 0.57	3 ± 3 [a] 23 ± 4 [b] 7.7 ± 0.9 [d]
^{142}Ce$(n,\gamma)^{143}$Ce	33 h	293.26	51.37	24	22.6 ± 1.1	19.6 ± 1.1	55 ± 9 [b]
^{175}Lu$(n,\gamma)^{176}$Lu^m	3.68 h	88.35	8.86 ± 0.25	24	906 ± 54		
^{176}Lu$(n,\gamma)^{177}$Lu	6.71 d	208.36	11.0 ± 0.4	24	1925 ± 95	1718 ± 85	2250 ± 200 [e]
^{181}Ta$(n,\gamma)^{182}$Ta	115 d	1121.0	34.86 ± 1.05	22	1192 ± 62	960 ± 50	981.7 [f]
^{197}Au$(n,\gamma)^{198}$Au	2.69 d	411.79	95.52 ± 0.06	accepted standard value for kT = 30 keV: 610 ± 15 [g]			

[a] Reference 9.
[b] Reference 17.
[c] Reference 16.
[d] Reference 14.
[e] Reference 18.
[f] Reference 13.
[g] Reference 11.

wellian averaged cross sections with only minor corrections. Especially neutron scattering caused large corrections in the recent measurements of Musgrove *et al.*[14] as was pointed out in Ref. 15 for the case of ^{140}Ce. This problem also caused the revision of the ^{138}Ba cross section.[14,16] As far as the results of Sidappa *et al.*[17] are concerned, we find in all cases discrepancies of a factor of 2 or even more which may be due to moderation effects in the perspex sample cannings. Also, a severe discrepancy was found for ^{140}Ce with respect to the cross section of Ref. 9.

For ^{176}Lu the result of Macklin and Gibbons[18] is 30% higher than our value. This relatively large cross section (with respect to ^{175}Lu) was interpreted in terms of theoretical arguments. However, another explanation might be that there is a shape problem in the data. If we extrapolate our cross section to higher energies using the energy dependence reported by Benzi *et al.*,[12] we find agreement with the data of Macklin and Gibbons above ~100 keV.

DISCUSSION

The Lu chronometer

In the mass region around ^{176}Lu fast and slow neutron capture are the main mechanisms for the synthesis of the chemical elements. Slow neutron capture (s process) forms the elements step by step along the valley of stability as it is shown in Fig. 5 by the solid line. Fast or rapid neutron capture (r process) is assumed to take place on the neutron rich side of nuclear matter. After the neutron flux has terminated the synthesized nuclei decay back to the valley of stability as is indicated in Fig. 5 by dashed arrows. ^{176}Lu is shielded against possible r-process contributions by its isobar ^{176}Yb. This means that ^{176}Lu was formed only by the s process. Therefore it is possible from s-process systematics to calculate how many ^{176}Lu was originally created. The comparison of that original abundance, $N^*(^{176}\mathrm{Lu})$ with the abundance $N(^{176}\mathrm{Lu})$ observed in the solar system offers then the possibility to evaluate the age of ^{176}Lu and herewith the age of the s process from the well-known ^{176}Lu half-life $T_{1/2}$ of 3.6×10^{10} yr. Although the production rate of s-process matter cannot be expected to be uniform in time, Schramm and Wasserburg[19] have shown that such fluctuations can be neglected if a long lived isotope like ^{176}Lu is used as a clock. Therefore a rather simple model can be applied in this case as it is discussed by Clayton[2] for the Re/Os chronometer. According to the definition of Ref. 2 the origin of time $t = 0$ is placed at the formation of the solar system 4.6×10^9 yr ago and t is measured backward in real time. If s-process nucleosynthesis began at a time T and decreased exponentially as $e^{\lambda t}$ then the abundance ratio of $N^*(^{176}\mathrm{Lu})$ and

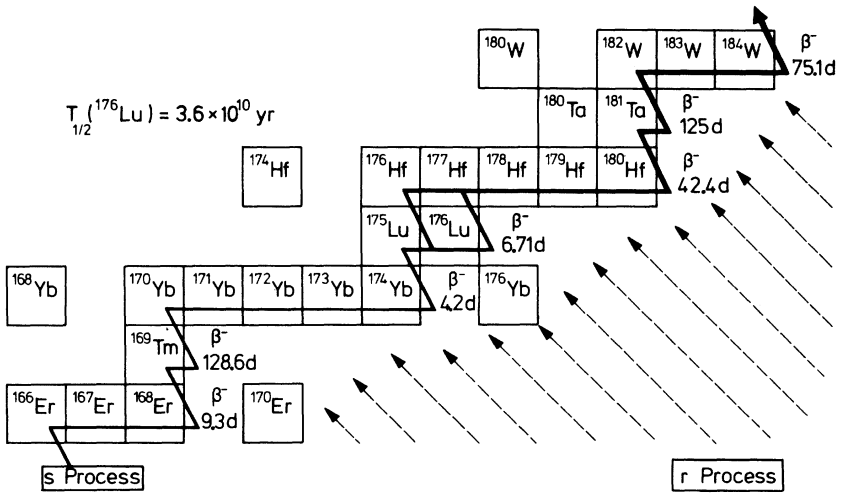

FIG. 5. The s-process synthesis path in the vicinity of ^{176}Lu (solid line). Possible r-process contributions are indicated by dashed arrows.

$N(^{176}\mathrm{Lu})$ can be written as

$$R=\frac{N^*(^{176}\mathrm{Lu})}{N(^{176}\mathrm{Lu})}=\frac{\Lambda-\lambda}{\Lambda}\,e^{\lambda T}\frac{1-e^{-\Lambda T}}{1-e^{-(\Lambda-\lambda)T}}\,, \tag{8a}$$

$$N^*(^{176}\mathrm{Lu}) = BN(176)\,. \tag{8b}$$

In Eq. (8a), $\lambda = \ln 2/T_{1/2}$ denotes the decay rate of ^{176}Lu. The factor B takes into account that only a fraction B of the total amount of synthesized nuclei $N(176)$ is formed in the ground state of ^{176}Lu. The residual part populates the 3.68-h isomeric state in ^{176}Lu which decays immediately to ^{176}Hf as it is shown in Fig. 6.

The time for the beginning of s-process synthesis T can be evaluated from Eq. (8a) if the ratio R is known. This requires the branching ratio B and the total abundance $N(176)$ at mass number 176. B is determined by the probability for populating the ground state via neutron capture in ^{175}Lu

$$B=\frac{\sigma^g(^{175}\mathrm{Lu})}{\sigma(^{175}\mathrm{Lu})}=1-\frac{\sigma^m(^{175}\mathrm{Lu})}{\sigma(^{175}\mathrm{Lu})}\,, \tag{9}$$

$\sigma^m(^{175}\mathrm{Lu})$, $\sigma^g(^{175}\mathrm{Lu})$, and $\sigma(^{175}\mathrm{Lu})$ are the Maxwellian averaged capture cross sections to the isomeric state and the ground state in ^{176}Lu as well as the total neutron capture cross section in ^{175}Lu, respectively. The total abundance $N(176)$ at mass number $A = 176$ must be derived from s-process systematics. Assuming an exponential flux distribution for the s process with a time integrated average flux τ_0, one obtains the following relation between the abundance $N(A)$ and the respective average capture cross section $\sigma(A)$[20]:

$$\sigma(A)N(A)=\sigma(A-1)N(A-1)\left[1+\frac{1}{\tau_0\sigma(A)}\right]^{-1}. \tag{10}$$

By means of this formula the product $\sigma(A)N(A)$ can be extrapolated from a stable s-process nucleus in the vicinity of ^{176}Lu to mass number $A = 176$ and $N^*(^{176}\mathrm{Lu})$ is then calculated using the experimental average capture cross section of ^{176}Lu.

The average flux τ_0 can be determined in the mass range around $A = 140$ where the magic neutron number 82 causes very small capture cross sections. In that range the σN values calculated with Eq. (10) are most sensitive to τ_0. Therefore, the cross sections of ^{138}Ba and ^{140}Ce were determined experimentally. For normalization of the calculated σN curve the abundance times cross section values of the pure s-process isotopes ^{148}Sm and ^{150}Sm were used.[21] These isotopes have the further advantage that also the abundance ratio of Lu and Sm is well defined due to the similar chemical behavior of both elements. In order to check the reliability of the theoretical σN curve, the calculation was performed in the entire mass range from ^{96}Mo to ^{190}Os. For most of the isotopes involved, experimental capture cross sections were used[13,14] except for the Xe isotopes and ^{160}Dy, where theoretical values from Benzi *et al.*[22] were taken.

The resulting σN curve is shown in Fig. 7 as a solid line. Obviously all pure s-process isotopes are fitted very well. In particular, the normalization at the Sm isotopes was extremely well confirmed by two recent cross section measurements

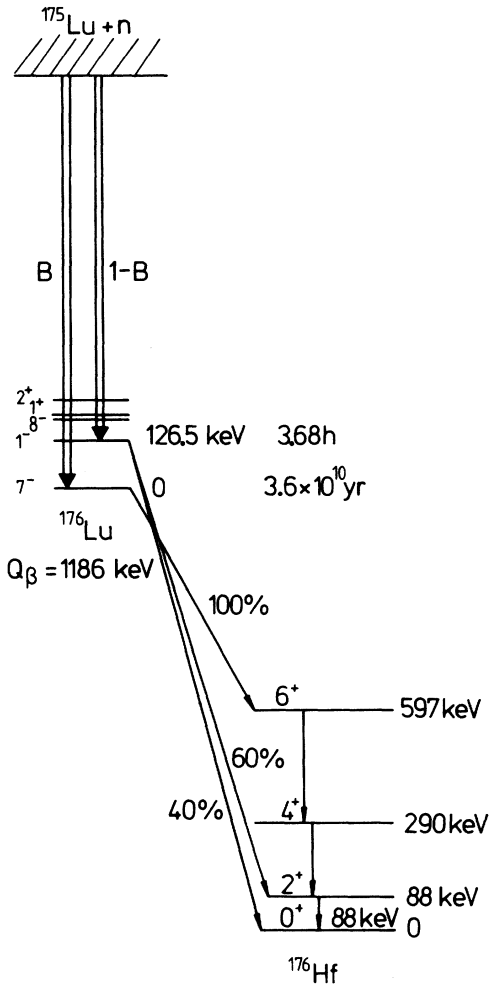

FIG. 6. The decay scheme of ^{176}Lu. The probabilities for populating the ground state (B) and the isomeric state (1-B) by neutron capture are indicated.

of ^{170}Yb (Ref. 23) and ^{186}Os (Ref. 24). Deviations from the calculated σN curve are observed only for ^{104}Pd and ^{110}Cd, which are not necessarily due to uncertainties of the respective cross sections, but may also be caused by the solar system abundance used for the evaluation.[25] The fact that the point for ^{176}Lu is much lower than the calculated curve is due to the branching ratio B and to the radioactive decay by about equal amounts.

The dotted and the dashed lines illustrate, how sensitive the σN curve depends on the cross sections of ^{138}Ba and ^{140}Ce as well as on the flux parameter τ_0. With our experimental cross sections and σN values of 6.1 ± 1.3 mb and 5.9 ± 1.15 mb (Si $\equiv 10^6$) for the normalization points at ^{148}Sm and ^{150}Sm, we find the best fit of the σN curve for $\tau_0 = 0.22$ mb^{-1}. This is in agreement with an earlier calculation of Shorin *et al.*[26] Apparently, the result of Ward *et al.*[27] who report a value of $\tau_0 = 0.25$ mb^{-1} is due to use of different cross sections for ^{138}Ba and ^{140}Ce.

As is obvious from Fig. 7 the σN curve is very flat above $A \sim 140$ with a slope almost independent of τ_0. Therefore the extrapolation of σN to ^{176}Lu is very reliable. To derive a best value for $N(176)$ the pure s-process isotopes ^{154}Gd, ^{170}Yb, ^{186}Os were used in addition to the Sm isotopes 148 and 150 to determine the σN value for $A = 176$ according to Eq. (10). With the resulting weighted average $\sigma N(176) = 4.89 \pm 0.12$ mb (Si $= 10^6$) R can be written as

$$R = \left[1 - \frac{\sigma^m(^{175}\mathrm{Lu})}{\sigma(^{175}\mathrm{Lu})}\right] \frac{\sigma N(176)}{\sigma(^{176}\mathrm{Lu}) N(^{176}\mathrm{Lu})} . \qquad (11)$$

In the present work, $\sigma^m(^{175}\mathrm{Lu})$, $\sigma(^{176}\mathrm{Lu})$, and τ_0 have been determined. For $\sigma(^{175}\mathrm{Lu})$ a value of (1411 ± 95) mb was adopted which is the weighted average of two experiments.[18,28] The abundances N are all taken from Cameron.[25] In Table IV, the quantities for the calculation of R which are taken from literature, are summarized. For the branching ratio the calculation yields $B = 0.43 \pm 0.05$ which is in excellent agreement with the theoretical value of 0.40 obtained by Shorin *et al.*[26] With the normalization points given in Table IV the weighted average of R is found to be $R = 1.13 \pm 0.15$.

The right-hand side of Eq. (8a) depends also on the s-process production rate for which two limits are evident:

(1) uniform synthesis with $\Lambda \to 0$ which yields
$$R = \lambda T/(1 - e^{-\lambda T}), \qquad (12a)$$

(2) sudden synthesis with $\Lambda \to \infty$ leading to $R = e^{\lambda T}$. (12b)

The assumption of a sudden synthesis gives a lower limit for T whereas a uniform synthesis results in an upper limit. As kind of an average between these limits, an exponentially decreasing production rate is assumed so that at the condensation of solar system the production rate has fallen to 9% of its initial value [$\Lambda = 1/(T \times 0.43)$].

Figure 8 shows the s-process age as a function of the ratio for all three assumptions on Λ. As can be seen immediately, T is sensitively dependent on R. Our results for the time from the beginning of s-process synthesis T are in excellent agreement with the values of Winters *et al.*[24] obtained from the analysis of the r-process chronometer ^{187}Re/^{186}Os. For the assumption $\Lambda = 1/(0.43 \times T)$ these authors obtain $T = 10.4 \times 10^9$ yr whereas we find $T = 9.5 \times 10^9$ yr.

It was pointed out in Ref. 19 that for long lived

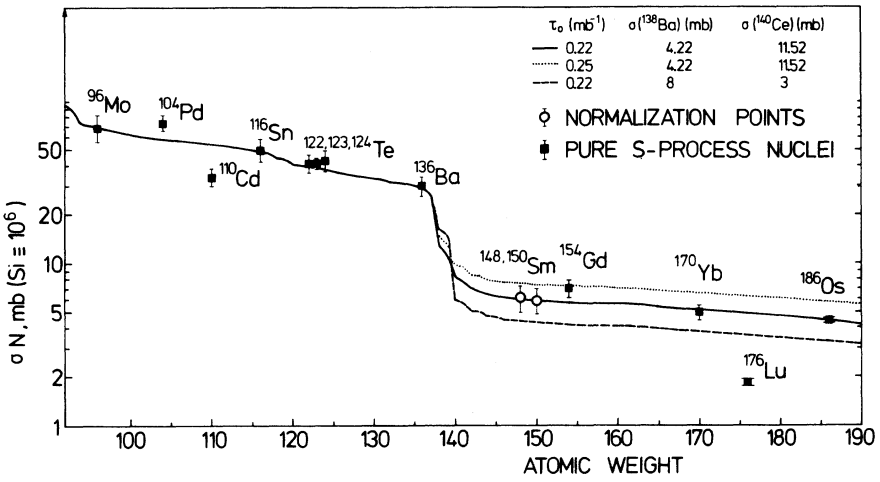

FIG. 7. The product of the Maxwellian averaged capture cross section σ times the s-process abundance N is plotted as a function of atomic number between ^{96}Mo and ^{190}Os. The sensitivity of the σN-curve with respect to the cross sections of ^{138}Ba and ^{140}Ce is demonstrated by the dashed line, whereas the dotted curve illustrates the influence of the flux distribution constant τ_0.

isotopes such as ^{176}Lu the solution of Eq. (12b) for a sudden synthesis yields not only a lower bound for the respective chronometer but represents also the mean age of s-process synthesis $\langle T \rangle$ independent of the history of the s-process production rate. Therefore this solution for $\Lambda \to \infty$ leads to an s-process age: $\langle T_s \rangle = (6 \pm 6) \times 10^9$ yr. The very large uncertainty of this value is mainly due to the uncertainty of the weighted average cross section of ^{175}Lu.

Although our result is not yet good enough for a real comparison it should be noted that it is consistent with the r-process age determinations of Winters *et al.*[24] and of Fowler and Hoyle.[1] The latter authors reported a value $T = (7 \pm 2) \times 10^9$ yr from an investigation of the ^{238}U/^{232}Th clock.

For a more accurate analysis of the ^{176}Lu chronometer it is clearly necessary to improve the accuracy of the relevant cross sections. This is certainly very difficult as at present an uncertainty

TABLE IV. Quantities for the evaluation of the s-process age T as taken from literature.

Isotope	s-process abundance N_S(Si≡10⁶)	$\frac{\langle \sigma v \rangle}{v_T}$(mb) (for kT = 30 keV)	$\prod_{i=A+1}^{176}\left(1+\frac{1}{\tau_0 \sigma(i)}\right)^{-1}$
^{148}Sm	0.0236 [a]	258 ± 48 [b]	0.819
^{150}Sm	0.0159 [a]	370 ± 72 [b]	0.832
^{154}Gd	0.00607 [a]	1164 ± 138 [c]	0.846
^{170}Yb	0.00622 [a]	790 ± 60 [d]	0.948
^{186}Os	0.00953 [a]	467 ± 12 [e]	1.097
^{176}Lu	0.00108 [a]		
^{175}Lu		1460 ± 110 [f]	
		1265 ± 190 [g]	
	weighted average	1411 ± 95	
$T_{1/2}(^{176}\text{Lu}) = (3.6 \pm 0.16) \times 10^{10}$ yr. [h]			

[a] Reference 25.
[b] Reference 29.
[c] Reference 31.
[d] Reference 23.
[e] Reference 24.
[f] Reference 18.
[g] Reference 28.
[h] Reference 13.

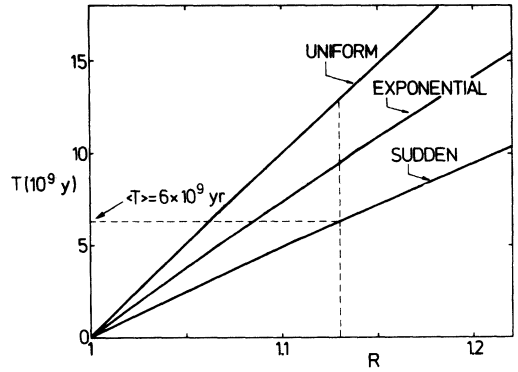

FIG. 8. The mean age T of the s-process isotopes as a function of the quantity R. Three models have been used for describing the time dependence of the synthesis (sudden, uniform, and exponential). The experimental result for R yields a mean age $\langle T\rangle = 6\times10^9$yr.

of 5% seems to be the state of the art for capture cross-section measurements in the keV region. The remaining possibility to achieve a better accuracy is to reduce the determination of R in Eq. (11) to the determination of cross section ratios only. Then, most systematic uncertainties cancel out and R might be obtained sufficiently accurately. Inserting Eq. (10) in Eq. (11) and rewriting this expression, one obtains

$$R=\left(\frac{\sigma(A)}{\sigma(^{176}\mathrm{Lu})}-\frac{\sigma^m(^{175}\mathrm{Lu})}{\sigma(^{176}\mathrm{Lu})}\,\frac{\sigma(A)}{\sigma(^{175}\mathrm{Lu})}\right)\frac{N(A)}{N(^{176}\mathrm{Lu})}\times\prod_{k=A+1}^{176}\left[1+\frac{1}{t_0\sigma(k)}\right]^{-1}. \tag{13}$$

Now R depends only on cross-section ratios. The important point is that $\sigma^m(^{175}\mathrm{Lu})$, the cross section to the isomeric state in ^{176}Lu, is combined with $\sigma(^{176}\mathrm{Lu})$ which can also be measured by activation. The other two ratios are to be determined by differential measurements. In principle, all isotopes listed in Table IV can be used as reference points as long as the respective abundance ratio $N(A)/N(^{176}\mathrm{Lu})$ is accurately known.

r - process abundances

The improved σN curve allows the evaluation of r-process contributions to the observed solar abundances for those isotopes where also accurate average cross sections are available. For the particular nuclei, which have been investigated in this work, the respective s- or r-process abundances are shown in Table V. For ^{138}Ba and ^{140}Ce our results are in fair agreement with the estimate of Suess and Zeh.[30] This is also true for N_r of ^{181}Ta, but as in this case Suess and Zeh assume a much lower value for the solar abundance of ^{181}Ta, their ratio N_s/N_r is significantly higher than our result.

The solar Hf abundance and the Hf/Zr ratio

In principle a determination of the age of the s-process T from the ^{176}Lu clock can also be performed with the s-only isobar ^{176}Hf. In this case the quantity R is given by the expression

$$R=\left[1+\frac{N(^{176}\mathrm{Hf})}{N(^{176}\mathrm{Lu})}\right]\Big/\left[1+\frac{1-B}{B}\,\frac{\sigma(^{176}\mathrm{Lu})}{\sigma(^{176}\mathrm{Hf})}\right]. \tag{14}$$

The difficulty in using ^{176}Hf for the ^{176}Lu clock is that the solar abundance of Hf obtained from meteorite analyses does not yield a consistent and unambiguous picture. This was pointed out by Arnould.[5] In view of this situation Arnould suggested, once the question of the age is settled, to evaluate the Hf abundance relative to Lu by means of Eq. (14). This represents a method independent from meteorite analysis and free from the uncertainties of chemical fractionation. With our value $R=1.13\pm0.15$ and a ^{176}Hf capture cross section $\sigma(^{176}\mathrm{Hf})=640\pm160$ mb (Ref. 9), we obtain from Eq. (14) $N(^{176}\mathrm{Hf})/N(^{176}\mathrm{Lu})=4.2\pm2.5$. This ratio and the solar ^{176}Lu abundance $N(^{176}\mathrm{Lu})=1.08\times10^{-3}$ from Ref. 25 yield $N(^{176}\mathrm{Hf})=(4.5\pm2.7)\times10^{-3}$ (Si $\equiv 10^6$) which is 41% of the ^{176}Hf abundance quoted by Cameron.[25] That means the Hf abundance must be corrected by that same factor in view of the new experimental results for B and $\sigma(^{176}\mathrm{Lu})$.

Due to the similar chemical behavior of Zr and Hf the abundance ratio Zr/Hf determined from meteorite analysis should be correct. With the Hf abundance normalized at ^{176}Lu, this yields an

TABLE V. r-process abundances derived from measured cross sections.

Isotope	σN from calculation (mb)(Si≡10^6)	$\frac{\langle\sigma v\rangle}{v_T}$ expt. (mb)	N_s (Si≡10^6)	N_{sol}[a] (Si≡10^6)	$N_r = N_{sol} - N_s$
^{138}Ba	12.88	4.22	3.05	3.44	0.39
^{140}Ce	8.20	11.52	0.71	1.04	0.33
^{181}Ta	4.75	960.0	5.0×10^{-3}	21×10^{-3}	16×10^{-3}

[a] All values from Ref. 25.

elemental Zr abundance of 12 ($Si \equiv 10^6$) which is also only 41% of the value given by Cameron.

ACKNOWLEDGMENTS

We appreciate very much that Dr. B. J. Allen, Dr. R. R. Winters, and Dr. J. Morel provided us with their results on ^{170}Yb, ^{180}Os, and $^{176}Lu^m$ prior to publication. Thanks are also due to H. Sobiesiak for the computer code and to the Van de Graaff staff for permanent assistance during the irradiations. We also thank Professor Schatz for valuable discussions.

[1]W. A. Fowler and F. Hoyle, Ann. Phys. (N.Y.) 10, 280 (1960).
[2]D. D. Clayton, Astrophys. J. 139, 637 (1964).
[3]J. Browne and B. Berman, Nature 262, 197 (1976).
[4]J. Audouze, W. A. Fowler, and D. N. Schramm, Nature Phys. Sci. 238, 8 (1972).
[5]M.Arnould, Astron. Astrophys. 22, 311 (1973).
[6]M. T. McCulloch, J. R. de Laeter, and K. J. R. Rosman, Earth Plan. Sci. Lett. 28, 308 (1976).
[7]W. R. Dixon, Nucleonics 8, 68 (1951).
[8]W. M. J. Veigele, At. Data Tables 5, 51 (1973).
[9]B. J. Allen, J. H. Gibbons, and R. L. Macklin, in *Advances in Nuclear Physics*, edited by M. Baranger and E. Vogt (Plenum, New York, 1971), Vol. 4, p. 205.
[10]J. Morel, CEA Saclay Report, No. LMRI-77-43/MJ, and private communication.
[11]ENDF/B IV Report BNL-17451 (ENDF-201), edited by D. Garber, National Nucl. Data Center, Brookhaven National Laboratory, Upton, New York (1975).
[12]V. Benzi, R. d'Orazi, G. Reffo, and M. Vaccari, C. N. E. N. Report RT/F1 (72) 6.
[13]M. J. Newman, Astrophys. J. 219, 676 (1978).
[14]A. R. de L. Musgrove, B. J. Allen, J. W. Boldeman, and R. L. Macklin, in *Proceedings of the International Conference on Neutron Physics and Nuclear Data, Harwell, 1978* (OECD Nuclear Energy Agency, Paris 1978), p. 449 A. R. de L. Musgrove, B. J. Allen, and R. L. Macklin, Aust. J. Phys. 32, 213 (1979).
[15]B. J. Allen, A. R. de L. Musgrove, R. L. Macklin, and R. R. Winters, in *Proceedings of the Specialists' Meeting on Neutron Data of Structural Materials for Fast Reactors, CBNM Geel, 1977*, edited by K. H. Böckhoff (Pergamon, New York, 1978), p. 506.
[16]A. R. de L. Musgrove, B. J. Allen, J. W. Boldeman, and R. L. Macklin, Nucl. Phys. A252, 301 (1975).
[17]K. Siddappa, M. S. Murty, and J. R. Rao, Nuovo Cimento 18A, 48 (1973).
[18]R. L. Macklin and J. H. Gibbons, Phys. Rev. 159, 1007 (1967).
[19]D. N. Schramm and G. J. Wasserburg, Astrophys. J. 162, 57 (1970).
[20]R. A. Ward, M. J. Newman, and D. D. Clayton, Astrophys. J. Suppl. 31, 33 (1976).
[21]R. L. Macklin, J. H. Gibbons, and T. Inada, Nature 197, 369 (1963).
[22]V. Benzi, R. D'Orazi, and G. Reffo, Nuovo Cimento 13B, 226 (1973).
[23]B. J. Allen and D. D. Cohen, Aust. J. Phys. (to be published).
[24]R. R. Winters, R. L. Macklin, and J. Halperin, Phys. Rev. C 21, 563 (1980), this issue.
[25]A. G. W. Cameron, Space Sci. Rev. 15, 121 (1973).
[26]V. S. Shorin, V. M. Gribunin, V. N. Kononov, and I. I. Sidorova, Astrofizika 7, 489 (1971).
[27]R. A. Ward and M. J. Newman, Astrophys. J. 219, 195 (1978).
[28]J. R. D. Lépine, R. A. Douglas, and H. A. Maia, Nucl. Phys. A196, 83 (1972).
[29]D. J. Horen and B. Harmatz, Nucl. Data Sheets 19, 410 (1976).
[30]H. E. Suess and H. D. Zeh, Astrophys. Space Sci. 23, 173 (1973).
[31]V. N. Kononov, B. D. Yurlov, E. D. Poletaev, and V. M. Timokhov, Yad. Fiz. 27, 10 (1978) [Sov. J. Nucl. Phys. 27, 5 (1978)].